J. Fluid Mech. (1966), *vol.* 24, *part* 4, *pp.* 823–843
Printed in Great Britain

Numerical experiments with free convection in a vertical slot

By J. W. ELDER

Institute of Geophysics and Planetary Physics, University of California,† San Diego

(Received 30 July 1965)

Numerical solutions of the equations of steady free convection in a vertical slot have been obtained by a procedure which relies solely on an iterative solution of Poisson's equation. With a mesh spacing of $\frac{1}{40}$ the solutions are stable up to a Rayleigh number of order 10^5. The numerical experiments are comparable to the author's laboratory experiments (Elder 1965) and to the experiments of Eckert & Carlson (1961). The growth of the boundary layers and the uniform vertical temperature gradient are well described. It is tentatively suggested that certain unstable motions found prior to the divergence of the numerical solution are comparable to the secondary flows found by the author.

1. Introduction

One of the more recent advances in theoretical fluid mechanics has been in the study of non-linear systems. Nevertheless, the analysis of many problems is in such a primitive state that our knowledge is largely restricted to that found in the laboratory. However, with present-day computing machines some of these problems can be studied with benefit both to the experimenter and theoretician. Already some fascinating studies have been reported (e.g. Fromm & Harlow 1963).

The aim of the present investigation is twofold. The immediate objective is an enquiry into the validity of the ideas about free convection in a vertical slot arising from some of the authors recent laboratory experiments (Elder 1965). The second and more long-term objective is the desire to construct a versatile computer programme to solve sets of simultaneous elliptic non-linear partial differential equations. The principal difficulty with such a task is that while numerical solutions can be readily generated their validity is generally not obvious. However, one can proceed by first solving problems that are well understood, adding additional features one at a time so that at each stage one has confidence in the solutions. Free convection in a porous medium is a particularly convenient starting point since the boundary conditions are the simplest ones possible, there is no diffusion of vorticity and the flow field is non-linear solely through the advection of heat. For a porous medium, the equations are (3*c*, *d*, *e*) below, together with the equation $w = A\theta_x$. The work with a porous medium will be reported in another paper. Given the porous medium programme we incorporate the additional parts (3*a*, *b*) which allow diffusion

† Now at Department of Applied Mathematics & Theoretical Physics, Cambridge.

and advection of vorticity appropriate to the flow of a viscous fluid. The evaluation of this problem and a comparison with laboratory experiment is the task of this paper.

Two things have principally contributed to this task. The first and most important has been laboratory experience with the system itself. The experimenter inevitably spends considerable time close to the experiment and even though many of his observations may not be immediately amenable to analytical discussion, he acquires a considerable familiarity with the behaviour of the system. The second matter has been some recent experience of the author with electronic analogue computers. These machines, designed to solve simultaneous non-linear ordinary differential equations give the user considerable insight into the behaviour of complicated non-linear servo-mechanisms. We find that the organization of a calculation such as that described here is closely analogous to the design of such servo-mechanisms.

In §§2 and 3 the numerical problem is formulated and the numerical procedure evaluated. The results are given in §4 followed by a discussion in §5. The calculations were performed on the CDC 3600 computer at the University of California, San Diego.

2. Formulation of the problem

2.1. *The systems of equations*

Consider the steady motion of a viscous fluid in a hollow rectangular prism of width L, height H, and breadth B, the vertical walls of which can be heated or cooled, while the top and bottom walls are insulators. Erect a co-ordinate frame O-XYZ with its origin in one corner of the prism. Let the vertical wall $x = L$ be maintained at temperature T_0, the wall $x = 0$ at temperature $(T_0 + \Delta T)$. If $B \gg L$ and H, the motion will be nearly everywhere two-dimensional, being confined to planes $y = \text{const}$. This problem has been studied theoretically by Batchelor (1954) and experimentally by Eckert & Carlson (1961) and Elder (1965).

For the purpose of the numerical calculations, replace the flow space by a finite number of points regularly spaced a distance D apart. Making the Boussinesq approximation, that density variations are significant only in their generation of buoyancy forces, and that other fluid parameters are independent of temperature, the problem is defined by: the kinematic viscosity, ν; the thermal diffusivity, κ; the acceleration due to buoyancy, $\gamma g \Delta T$ where γ is the coefficient of cubical expansion; the width L; the height H; and the mesh spacing D. Hence since these involve only the dimensions of length and time, four dimensionless parameters are needed to specify the system. A convenient set is:

$$\left.\begin{aligned} \sigma &= \nu/\kappa && \text{Prandtl number;} \\ A &= \gamma g \Delta T L^3/\kappa\nu && \text{Rayleigh number;} \\ h &= H/L && \text{Aspect ratio;} \\ d &= D/L && \text{Mesh spacing.} \end{aligned}\right\} \tag{1}$$

The field variables can be conveniently made dimensionless by choosing *units* of length, temperature, pressure, velocity:

$$L, \Delta T, \rho_0 Lg, \kappa/L. \tag{2}$$

The dimensionless temperature will be written as θ. We shall write $\bar{x} = 1 - x$. Note that the choice of velocity unit follows Batchelor (1954) rather than Elder (1965).

For steady, two-dimensional flow the field equations, simplified by the Boussinesq approximation, can be written with the units (2) in the dimensionless form (Batchelor 1954)

$$U = -A\theta_x + (1/\sigma)\,\partial(\psi, \omega), \tag{3a}$$

$$\nabla^2\omega = U, \tag{3b}$$

$$\nabla^2\psi = \omega, \tag{3c}$$

$$V = \partial(\psi, \theta), \tag{3d}$$

$$\nabla^2\theta = V, \tag{3e}$$

where ∂ is the Jacobian operator and x is the horizontal co-ordinate. Note that the velocity $\mathbf{q} = (-\psi_z, \psi_x)$ and the vorticity $\boldsymbol{\omega} = \nabla \times \mathbf{q} = -\hat{\jmath}\omega$, where $\hat{\jmath}$ is a unit vector parallel to the y-axis (into the paper in the diagrams shown here). The source terms U, V are the rate of generation of vorticity and temperature. Vorticity is generated by the torque arising from the horizontal gradient of the buoyancy forces. Otherwise U, V are produced by advection. In the discussion $\partial(\psi, \omega)$ will be called the inertia and $\partial(\psi, \theta)$ the advection.

Equations (3) are to be represented by finite differences at the mesh points. The methods of obtaining this representation can be found in the standard texts (e.g. Fox 1962). Henceforth we regard (3) merely as a convenient shorthand for this finite-difference representation.

2.2. *Numerical method*

Numerous schemes have been proposed and used for the numerical solution of systems of equations such as the above. All of these schemes are equivalent to the inversion of a large sparse matrix by an iterative procedure. The method used here uses the equations as written in (3). Test functions $U(0), \omega(0), \psi(0), V(0), \theta(0)$ are first chosen and then each equation is solved in turn in the cycle $(a, b, c, d, e, a, \ldots)$ until the solution has converged or the process is terminated when the solution begins to diverge. Such a sequential scheme has the merit that the solution develops in a similar manner to that of the time-dependent problem at large times (cf. Garabedian 1956). The initial, high wave-number transients of the time-dependent problem do not appear. The method is very straightforward, the only point of departure from other authors is the treatment of the vorticity equation and the isolation of the non-linear terms.

With respect to the vorticity equation one has the choice of solving the biharmonic equation, $\nabla^4\psi = U$ or, as here, solving Poisson's equation twice. Without an elaborate investigation, there is no clear choice. However, numerical schemes for solving the biharmonic equation are notoriously slowly convergent. For meshes of size 10×10 to 40×40 the double Poisson method has been

found to be much more rapid than the direct solution of the biharmonic equation. (A single application of the biharmonic 'molecule' takes more than twice the time of that for the Poisson 'molecule'.) The outstanding advantage of the double Poisson method is that the optimization of the iteration of Poisson's equation is well understood. The only disadvantage is the loss of computer memory to store ω.

The isolation of the non-linear terms is very convenient and has produced no obvious difficulties. The bulk of the calculation is thereby spent solving Poisson's equation, a process which can be made very rapid. In schemes which incorporate the non-linear terms into the relaxation molecule it is difficult to choose an optimum relaxation scheme and the origin and development of numerical instabilities is obscured. The essential interest in such calculations is the role of the non-linear terms, here made as explicit as possible.

3. Evaluation of the numerical scheme

The basic assumption of § 2 is that the solutions of the finite-difference scheme tend to the 'analytic' solution as $d \to 0$. However, in practice only a small number of mesh points can be used (the smallest value of d used here was $\frac{1}{80}$), so that it is necessary to determine by experiment whether or not the numerical solution corresponds to the analytic solution. This is especially difficult when no suitable analytic solutions are known. One must, therefore, check each operation of the numerical procedure and where possible compare the results with suitable laboratory experiments. The former task will be discussed here, the latter in subsequent sections.

Four major matters are strongly controlled by d: (i) stability; (ii) speed of convergence; (iii) precision, viz. number of significant figures of converged solution; (iv) accuracy, viz. departure of the numerical from the analytic solution. To summarize the results for the above scheme:

(i) For example, given σ and h the solution will rapidly diverge for values of $A \propto 1/d^2$.

(ii) The speed of convergence $\propto d^2$.

(iii), (iv) Precision and accuracy are of order d^2. These are the predictions of numerical analysis (Fox 1962).

3.1. *On the solution of Poisson's equation*

There is a vast literature on the problem of finite-difference methods of solving Poisson's equation. Fortunately the problem is sufficiently well understood for one to proceed in a simple-minded way. The superiority of Liebmann's extrapolated method is well known (Fox 1962). For example, if

$$\nabla^2 \psi = \omega, \tag{4}$$

where ω is given and there are suitable boundary conditions on ψ, we have the finite-difference scheme

$$\psi(i,j) = G\psi(i,j) - C\omega(i,j) + B[\psi(i+1,j)+\psi(i-1,j)+\psi(i,j+1)+\psi(i,j-1)]. \tag{5}$$

The system of equations is scanned row by row or column by column using 'new' values where present. In the 'ordinary' method $G = 0$, $B = \frac{1}{4}$, $C = \frac{1}{4}d^2$. The values used in the 'extrapolated' method are for a high degree of over-relaxation. They are

$$G = 1-E, \quad B = \tfrac{1}{4}E, \quad C = \tfrac{1}{4}Ed^2, \tag{6a}$$

where

$$E = 2\{1-(1-T)^{\frac{1}{2}}\}/T, \tag{6b}$$

and

$$T = 0{\cdot}5[\cos(\pi/m)+\cos(\pi/n)], \tag{6c}$$

for a mesh $(m+1) \times (n+1)$.

If one is merely interested in the solution of Poisson's equation alone, there is at first sight little to choose between various ways of scanning the equations. However, it is soon apparent in a system of equations involving non-linearities that numerical instabilities readily arise and that the onset of these is very dependent on the scanning method. There are, of course, eight possible ways of combining row, column, and direction of scan. Liebmann's method uses only one of these and thereby accumulates the errors in one corner. It is much better to alternate row, column and direction of scan. The error is then more evenly distributed and most important the *form* of the solution emerges much more rapidly. For a mesh much longer in one dimension than the other it is found best to scan only across the smaller dimension; there are then only four possible ways of scanning. Such a sequence of four iterations will be called a 4-scan. This method is rather similar to a method of Peaceman & Rachford (1955).

As an example, consider the rectangle

$$x = 0-2, \quad z = 0-1 \quad \text{with} \quad \omega = \sin 2\pi x \sin \pi z$$

and $\psi = 0$ on the boundary. The ordinary method is very slow, requiring more than 50 iterations. Liebmann's extrapolated method has a very rapid initial approach to the final solution. We notice that there is a slight overshoot and a subsequent damped oscillation about the final solution. The alternating row, column, direction method is a little slower, but has no perceptible overshoot. In the language of servo-mechanisms the system is nearly critically damped. Both the Liebmann methods have converged to within 0·1 % in a 41×21 mesh after 40 steps, to the centre value of 0·02042. The analytic value is $\frac{1}{5}\pi^2 = 0{\cdot}02026$. The numerical values are therefore 0·8 % high. The form of the solution with the alternating system is very much the best; the form after only one 4-scan is superior to that of the Liebmann extrapolated method after 20 iterations.

It is seen that the rate of convergence rapidly falls as the final solution is approached. This may appear to be an unfortunate (and expensive) situation. Actually this proves to be a great advantage since, as shown in figure 1, if ψ_∞ is the final solution, approximately,

$$\psi_\infty - \psi \propto e^{-\lambda s}, \tag{7}$$

where s is the number of iterations and λ is a constant. Hence given 3 successive values of ψ we can estimate ψ_∞ from

$$\psi_\infty = (\psi_2^2 - \psi_1\psi_3)/(2\psi_2 - \psi_1 - \psi_3). \tag{8}$$

This method is similar to one used in some relaxation calculations (Aitken's method). It is here that the method of alternating row, column, direction has its advantage. Since the form of the solution emerges rapidly, it is only necessary to use the maximum absolute value of ψ at 3 successive stages to calculate the extrapolation factor. A near optimum method is to choose these three values to be the starting value and the two values after two 4-scans. Thus a single

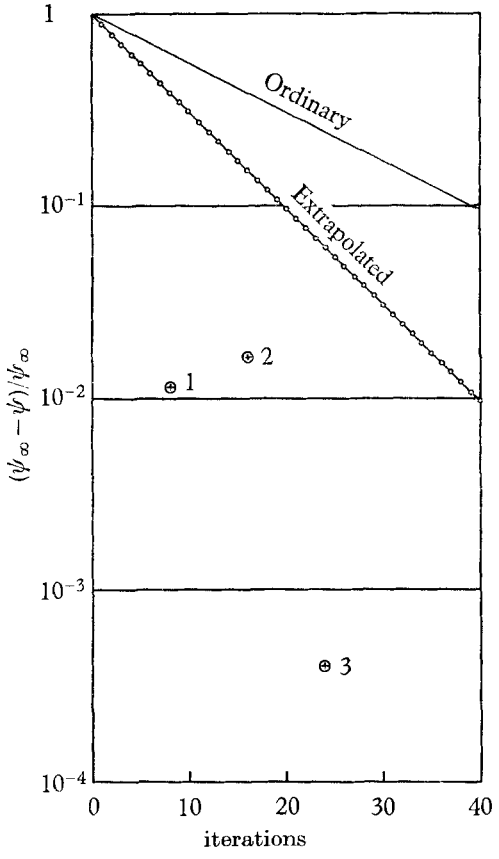

FIGURE 1. Convergence of the iterative solution of Poisson's equation: departure of the value which is a maximum over the mesh. Also shown are the values for three successive extrapolations.

extrapolation involves 8 iterations. Included in figure 1 are the values obtained after 3 successive extrapolations. The improvement after the first extrapolation is particularly marked: the error is 30 times smaller than for the non-extrapolated value, alternatively the time to reach about 1 % accuracy has been reduced by a factor of 5. (Incidentally, an error of 1 % requires 10 times as many iterations with Liebmann's ordinary method.) It should be noted that the extrapolation method is stable, repeated extrapolations do not produce any difficulty (10 successive extrapolations was the largest number tested). Table 1 is a summary of the solutions of (4) with $\omega = \sin \pi x \sin \pi z$ and $\psi = 0$ on the boundary of a square cavity after 10 extrapolations. It is seen that a satisfactory solution for $1/d = 10$,

20, 40, 80 is obtained after 1, 3, 5, 7 extrapolations since for these the error in the solutions is less than the absolute error. The corresponding time of calculation on the CDC 3600 including output of the solution is about $1{\cdot}2 \times 10^{-2}/d^2$ sec. This figure proves to be a good estimate of the computation time for all the solutions reported here.

	Extrapolations							
Mesh	1	2	3	4	5	6	7	Absolute error
11×11	0·16	0·32	0·00	—	—	—	—	0·84
21×21	1·36	1·88	0·04	0·00	0·00	0·00	—	0·20
41×41	4·28	4·68	0·88	0·16	0·04	0·00	—	0·04
81×81	8·76	9·12	4·24	1·56	0·24	0·04	0·00	0·01

TABLE 1. Departure from numerical solution (i.e. after 10 extrapolations) of maximum value of solution of Poisson's equation in percentages. The absolute error is for the maximum value.

3.2. *The boundary conditions*

The treatment of the boundaries is simplest for (3*e*). On the vertical walls the temperature is given so that only interior points are considered. On the ends, we will choose $T_z = 0$ so that we require at the boundary points a molecule in which the value at the image point is equal to that at the interior point (central difference of $T = 0$). The end wall points are swept only in the direction of the flow. I have not found any difficulty due to this simplification.

In (3*c*) $\psi = 0$ on the walls, so that the simplest procedure is to regard all points as simple interior points except for those immediately adjacent to the wall. For these points we assume, as in the boundary-layer approximation, that diffusion near the wall is predominantly normal to the wall and evaluate

$$\psi' = \tfrac{1}{2}d^2\omega', \tag{9}$$

where ψ' and ω' are the values at points adjacent to the boundary. This relation ensures that the normal derivate of ψ is zero to order d^2.

Equation (3*b*) has not been quite so straightforward. There has been no difficulty on the vertical walls where a similar device to (9) is used. We evaluate

$$\omega = d^2U + 2\omega' - \omega'', \tag{10}$$

where ω', ω'' are evaluated at x, $\bar{x} = d$, $2d$. This expression is also accurate to order d^2. Application of this relation on the ends, however, leads to pronounced numerical instability. I have tried numerous devices including linear, quadratic and cubic extrapolation and various relaxation molecules without much success. The most stable was found to be $\omega_z = 0$. This is rather an artificial condition. Fortunately, the error introduced is small and for the problems discussed here the ends are not the region of principal interest. In the computation we simply place $\omega = \omega'$ after each interior scan.

Notice in the above scheme that boundary conditions are applied directly and *not by relaxation* except that relaxation is used in (3*e*) on the ends.

It is also apparent that the solution ω of (3*b*) contains an arbitrary harmonic function ϕ. With the alternating row, column, direction scheme we find experimentally that ϕ is nearly uniform over the mesh and increases with the number of iterations. This artifact of the double Poisson method can be suppressed, therefore, noting from Stokes's theorem, since the velocity is zero on the walls, that the mean vorticity over the mesh must be zero, by subtracting the mean vorticity from each mesh value at the end of each 4-scan. This adds a negligible amount to the time of computation.

3.3. *Verification of the double Poisson method by solution of the biharmonic equation*

An interesting test case for the double Poisson scheme is the problem

$$\nabla^4(\psi/A) = 1 \tag{11}$$

in a rectangle of unit width and height h with $\nabla\psi = 0$ on the walls (see e.g. Batchelor 1954; Love 1927, chapter 22). This is the solution of (3), for finite σ, as $A \to 0$. Table 2 gives values of $\psi_{\max}$ and $\omega_{\max}$ for various h and compares them with values estimated by Love (1927). The rather artificial boundary condition applied to ω on the ends strongly constrains ω to take (here) its value for $h \to \infty$. This leads to a significant but acceptable error in ψ and is a reasonable price to pay for rapid convergence and stability.

		Present work		After Grashoff		Error	
Mesh	h	$\psi_{\max}$	$\omega_{\max}$	$\psi_{\max}$	$\omega_{\max}$	$\psi_{\max}$	$\omega_{\max}$
11×41	4	$3{\cdot}13 \times 10^{-3}$	$8{\cdot}00 \times 10^{-2}$	$2{\cdot}59 \times 10^{-3}$	$8{\cdot}30 \times 10^{-2}$	$+21\,\%$	$-3{\cdot}6\,\%$
11×21	2	$2{\cdot}92 \times 10^{-3}$	$7{\cdot}93 \times 10^{-2}$	$2{\cdot}45 \times 10^{-3}$	$7{\cdot}84 \times 10^{-2}$	$+19\,\%$	$+1{\cdot}1\,\%$
11×11	1	$1{\cdot}75 \times 10^{-3}$	$7{\cdot}83 \times 10^{-2}$	$1{\cdot}30 \times 10^{-3}$	$4{\cdot}17 \times 10^{-2}$	$+35\,\%$	$+88\,\%$

TABLE 2. Numerical solution of the biharmonic equation with $\omega_z = 0$ on $z = 0, h$ compared with the heuristic formula of Grashoff (Love 1927).

3.4. *The 'outer' iteration*

The organization of the steps (a, b, c, d, e, a, ...) has been called the 'outer' iteration. This part of the problem is much less well understood than the 'inner' iterations. I have found it particularly helpful to consider the problem analogous to that of the design of servo-mechanisms. The criteria for stability and rate of convergence are very similar. The method used here has however been determined by experiment. It is not necessarily the best.

The calculation proceeds thus (in an obvious notation): given U_0, θ_0 etc. find:

$$\omega_1(U_0), \psi_1(\omega_1), U_1(\theta_0, \psi_1, \omega_1), \omega_2(U_1), \psi_2(\omega_2);$$
$$V_1(\psi_2, \theta_0), \theta_1(V_1), V_2(\psi_2, \theta_1), \theta_2(V_2);$$
$$U_2(\theta_2, \psi_2, \omega_2), \ldots$$

and so on. Note that each solution of Poisson's equation involves one 4-scan (i.e. 4 iterations), so that a scan of (3) involves 8 iterations of each of the Poisson equations.

Two modifications of this scheme have been used. First, if one is interested in only a single value of the parameters, one may use the extrapolation scheme, described above. I found this useful only once, at the beginning of the calculation. Repeated extrapolations easily lead to instability. (A critically damped non-linear servo-mechanism will often become unstable if the damping is reduced.) Secondly, a very helpful device is to change the parameters after each scan. For example one may take $A_s = A_0 + s\Delta A$, where $s = 1, 2, 3, \ldots, n$ is the number of scans and $\Delta A/A \ll 1$. With the present scheme, values of $\Delta A/A$ as large as 0·05 are convenient. It is interesting to note that numerical instability occurs at rather higher values of A with this scheme (the improvement is generally about a factor of 2). The results given below, unless otherwise stated, use this scheme, the form of the ramp being indicated in the usual way as $A_0(\Delta A)\, A_n$.

3.5. *Stability of the 'outer' iteration*

In all the experiments performed here tests were first performed to determine the range of the parameters for which a stable, reasonably precise solution was possible. All of these showed the behaviour illustrated in figure 2, which shows a suitable parameter, here the Nusselt number

$$N \equiv -\frac{1}{2h}\int_0^h [\theta_x(0,z) + \theta_x(1,z)]\, dz,$$

for $\sigma = 1$ and a 11×11 mesh at various A, as a function of the number of 4-scans. For $A \lesssim 4200$ the solution is stable. The initial transient behaviour is typical of an under-damped servo-mechanism. It is seen that the damping decreases as A increases. However, for somewhat larger values of A the solution is no longer stable. As shown, at $A = 4250$ the solution begins to diverge at scan number 30. Beyond this point the solution amplitude grows super-exponentially so that after a few more scans overflow occurs on the computer. The critical condition is surprisingly sharply defined.

For solutions using a ramp it was found that the critical condition occurred at a somewhat higher A, but never higher by more than a factor of 2. This suggests that the outer iteration could be further improved.

3.6. *Precision*

The data from a typical test of the precision obtainable are shown in table 3 for a 40-step calculation for flow in a square cavity with $A = 10^3$, $\sigma = 1$. It is seen that the values for N are more precise than those of U and V. For example, with a 41×41 mesh the precision of $\psi_{\max}$ and N is of order 0·1 % whereas for U and V it is 1 and 4 %. The values even for the 11×11 mesh are quite acceptable, but there is a marked improvement in the 21×21 mesh. Except for calculations at the highest Rayleigh numbers, there is little to be gained from larger meshes.

4. Results of the numerical experiments

The numerical experiments have partially explored the region:

$$\sigma = 10^{-2}\text{–}10^4, \quad A = 0\text{–}5 \times 10^4, \quad h = 0{\cdot}5\text{–}8, \quad d = \tfrac{1}{10}\text{–}\tfrac{1}{80}.$$

A selection from stable solutions is presented below. The results cover a somewhat different region from those of the author's experiments (Elder 1965), where most of the measurements were for $A > 10^4$ and $h \approx 10$. They do, however,

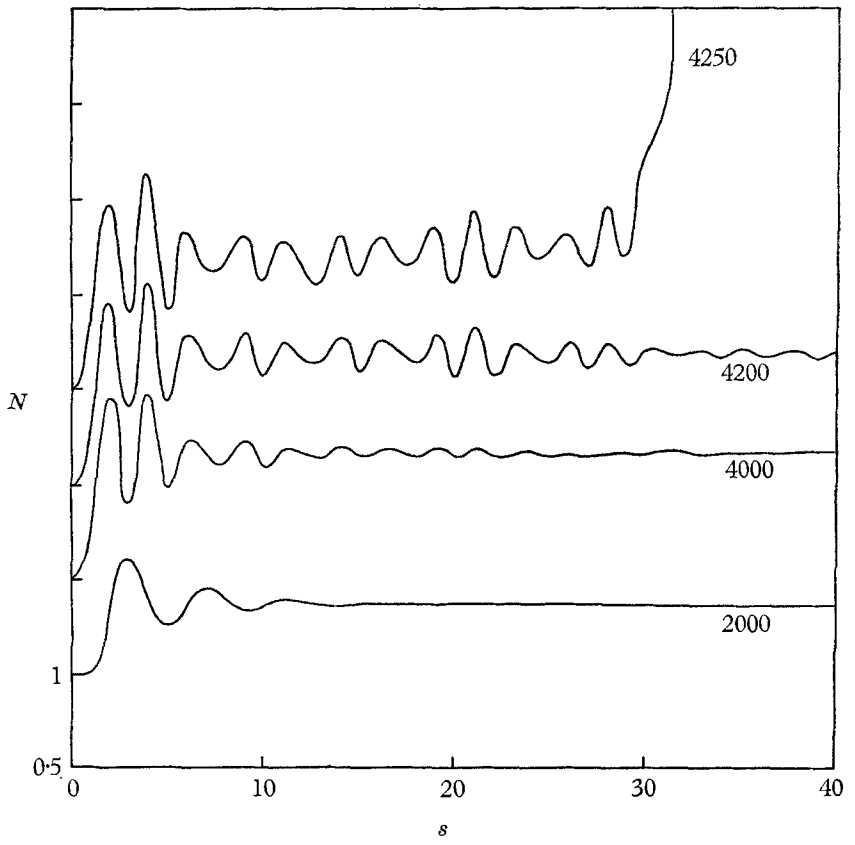

FIGURE 2. Stability of the outer iteration at various Rayleigh numbers A with $\sigma = 1$. Nusselt number N at scan s on a 11×11 mesh. Curves displaced vertically 0·5.

Mesh	ψ_{max}	N	ω_{max}	U_{max}	V_{max}
11×11	2·412	1·378	132	6180	11·1
21×21	2·562	1·472	128	7250	13·3
41×41	2·558	1·475	137	7570	14·4
$d = 0$	2·560	1·475	137	7660	15·0

TABLE 3. Precision test, $A = 1000$, $\sigma = 1$, 40 scans. The $d = 0$ values are estimates.

cover a similar range to the excellent measurements of Eckert & Carlson (1961). The reader is recommended to inspect their paper while studying the present solutions.

It has been found that h does not greatly affect the *form* of the solution. Therefore, except for the data of figure 5, the discussion will be restricted to flow in a square. Should the reader desire to obtain an approximation to the flows in a

rectangle with $h \neq 1$ he should simply apply the transformation $z' = hz$, $A' = A/h$ (Elder 1965) to the various distributions given for a square.

Unfortunately the solutions are very unstable for small values of the Prandtl number. Below $\sigma \approx 0{\cdot}1$ the solutions are stable only in the linear region so that no new information is available; above $\sigma \approx 1$, the Prandtl number has only a minor effect. A direct investigation of the role of σ is given in §4.6. Otherwise, the solutions are for $\sigma = 1$.

A few remarks on the presentation of the results is necessary. Several of the figures show the variation of a quantity within the cavity. The name of the quantity and its maximum absolute value are written on the figures. The lines

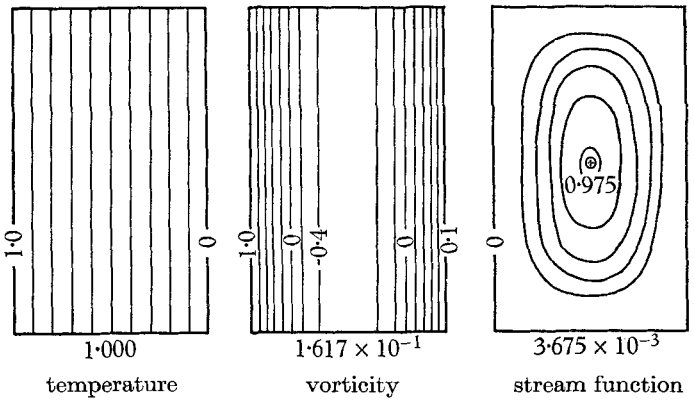

FIGURE 3. Weak convection in a square cavity. Temperature, vorticity and stream function for $A = 2$, $\sigma = 1$, $h = 1$ and mesh 21×21. (Note: in these figures the vertical scale is $\frac{5}{3}$ of the horizontal scale.)

are drawn at intervals $-1\ (0{\cdot}2)\ 1$ of the maximum absolute value. However, where the quantity varies rapidly all the lines may not be shown. For example, in figure 7(f) only the contours $-0{\cdot}4\ (0{\cdot}2)\ 0{\cdot}4$ are shown. Occasionally other labelled contours will be shown. It is important to note in all such figures that the vertical scale is $\frac{5}{3}$ of the horizontal scale—this was dictated by the system used to output the distributions directly onto the line printer. Finally, note that in all these figures the left-hand wall is the hot one.

4.1. *The flow as* $A \to 0$

For A sufficiently small, the flow approaches the solution of the linear problem $\theta = 1 - x$, $\nabla^4\psi = A$ (Batchelor 1954). Figure 3 shows θ, ω, ψ for $A = 2$, $\sigma = 1$ for a square cavity. We notice that the temperature is indistinguishable from $\theta = 1 - x$. The vorticity is independent of z because of the artificial boundary condition $\omega_z = 0$ on the ends (see §3.2). The distribution and amplitude of ω and ψ are indistinguishable from those calculated in §3.3 directly from (11).

Figure 4 shows the terms neglected in the linearization, viz. the advection and the inertia. Notice that the form of the advection is similar to $\sin \pi x \sin 2\pi z$, while the form of the inertia is similar to $\sin 2\pi x \sin 2\pi z$. This feature of V having

two regions of opposite sign, and U having four regions of alternating sign will be found to persist to high Rayleigh numbers.

The non-linear terms arise in the end regions. This is clearly shown in figure 5 which gives V for $h = 1, 2, 4$ at $A = 2$, $\sigma = 1$. It is apparent that the end regions

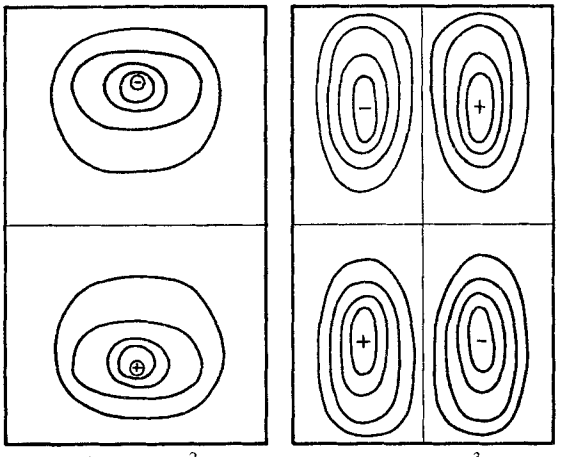

FIGURE 4. Advection and inertia for $A = 2$, $\sigma = 1$, $h = 1$ and mesh 21×21 (as in figure 3).

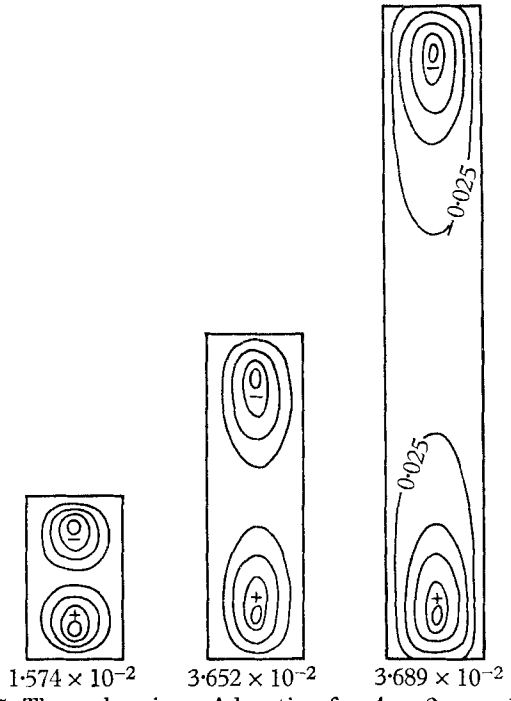

FIGURE 5. The end regions. Advection for $A = 2$, $\sigma = 1$, $d = \frac{1}{10}$ and $h = 1, 2, 4$.

at low Rayleigh numbers extend a distance of order L into the cavity (cf. Eckert & Carlson 1961, figure 2(*b*)).

4.2. *Development of the boundary layers*

For small values of A the non-linear terms play a negligible role in the motion. The flow is maintained solely by a balance between viscous forces and buoyancy forces. We notice that the vorticity source strength $U \doteqdot A$ has the same value everywhere. However, as A is increased the motion becomes increasingly dominated by the non-linear terms. This is most strikingly illustrated by the

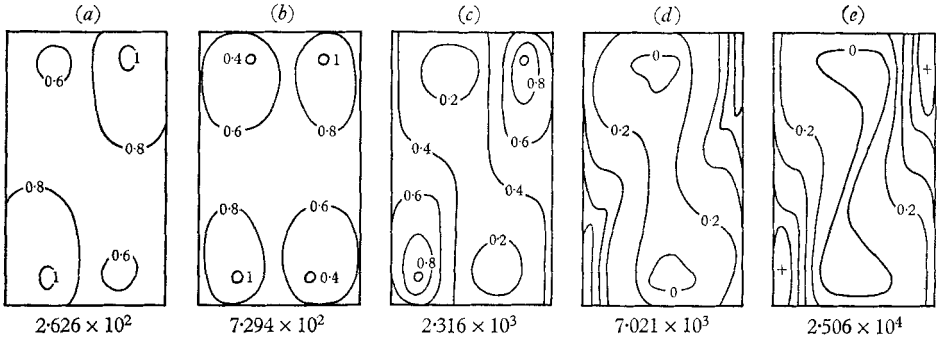

FIGURE 6. Development of the boundary layers. The vorticity source term U at A: (*a*) 200, (*b*) 500, (*c*) 1000, (*d*) 2000, (*e*) 5000; for $\sigma = 1$ and a 21×21 mesh.

growth of U. Figure 6 shows U for a sequence of Rayleigh numbers. The first departure from uniformity of U is the more rapid growth of U in the lower left-hand and the upper right-hand corner, producing a saddle in the middle of the cavity (see $A = 200, 500$ in figure 6). At $A \approx 1000$ the lower left and upper right regions have become more pronounced and negative values of U are about to appear (values of $U < 0$ are present at $A = 1050$). The distribution of U now becomes increasingly localized near the vertical walls with an increasingly gentle depression between them (see $A = 2000, 5000$ in figure 6). As we shall see more clearly below, the solutions of figure 6 span the region from that of a linear system to that of boundary-layer flows.

The solution for a fully-developed boundary-layer flow is shown in figure 7. The localization of the non-linear terms, the inertia and the advection, to the vicinity of the vertical walls is pronounced and both the vorticity and the temperature show strong horizontal gradients in the boundary-layer regions near the vertical walls. The uniformity of the distributions in the interior is striking. In particular the negligible vorticity and the nearly uniform vertical temperature gradient in the interior confirms the prediction of Elder (1965). Another striking feature is the marked collapse of each boundary layer beyond its point of maximum growth at $z = \frac{1}{2}h$, indicating that the fluid is no longer being accelerated by the dominance of buoyancy forces over viscous forces. This is seen in the localization of the inertia and the advection to the growing part of the layer (lower left-hand and upper right-hand walls) and the more rapid growth of the thermal and vorticity layers beyond $z = \frac{1}{2}h$ (upper left-hand and lower right-hand

walls). In Elder (1965) it was suggested that this process could be interpreted as a competition between the two layers to entrain interior fluid.

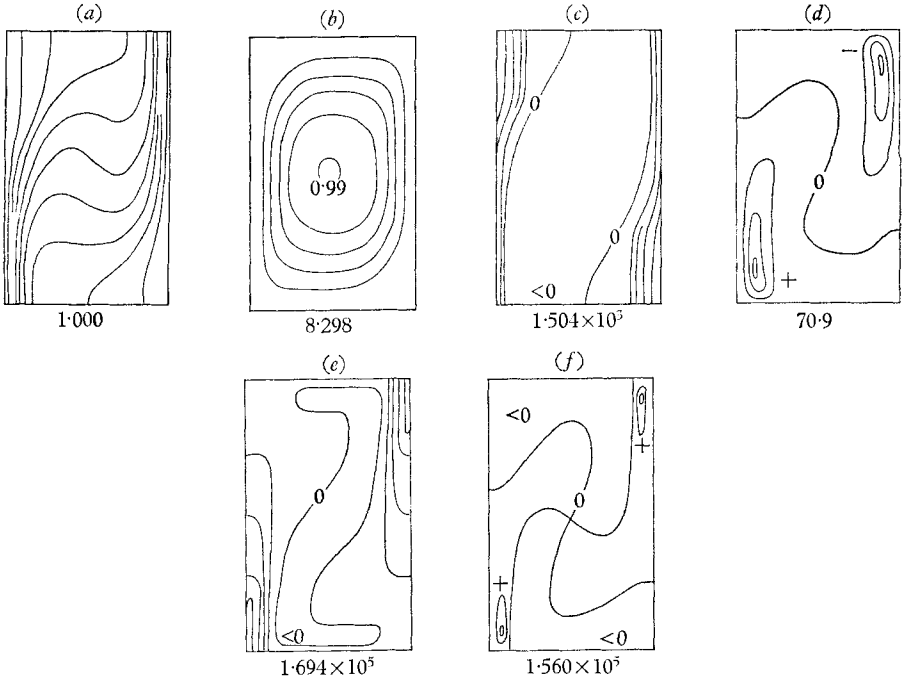

FIGURE 7. Boundary-layer flow at $A = 2 \times 10^4$, $\sigma = 1$ for a 41×41 mesh: (*a*) T, (*b*) ψ, (*c*) ω, (*d*) V, (*e*) U, (*f*) $\partial(\psi, \omega)$.

4.3. *The maximum value of the stream function*

Figure 8 shows values of $\psi_{\max}$ as a function of A. Two distinct regions are observed:

$$\psi_{\max} = 1{\cdot}70 \times 10^{-3} A \quad (A < 200), \tag{12a}$$

$$\psi_{\max} = 5{\cdot}87 \times 10^{-2} A^{\frac{1}{2}} \quad (A > 10^3). \tag{12b}$$

These forms are to be expected. The linear region, in which $\psi \propto A$ has been predicted by Batchelor (1954) by considering the flow as $A \to 0$. The values are somewhat higher than predicted. This is undoubtedly due to the boundary condition applied here on the ends (see §3.2). The non-linear region in which $\psi \propto A^{\frac{1}{2}}$ indicates the presence of thermal boundary layers, as obtained for example in Squire's calculation (Goldstein 1938). It was somewhat surprising that the non-linear region could be demonstrated in very small meshes (viz. $d = \frac{1}{10}$).

The approach of the solution to the steady-state solutions is indicated on the figure for various ramps. Note that if ΔA is sufficiently large, there is a small overshoot.

4.4. *The heat flux*

Figure 9 shows the Nusselt number N as a function of A. Again there are two distinct regions, corresponding to those of figure 8

$$N \doteq 1, \tag{13a}$$

$$N/A^{\frac{1}{4}} = 0{\cdot}25 \pm 0{\cdot}01, \quad A > 4000, \quad h = 1. \tag{13b}$$

4.5. *The vertical temperature gradient*

One of the intriguing features of free convection in a vertical slot is the growth of a uniform non-zero vertical temperature gradient $\beta \equiv \theta_z(\frac{1}{2}, \frac{1}{2}h)$ (Elder 1965). Figure 7 (*a*) shows the temperature distribution for $A = 2 \times 10^4$. In the central region of the cavity the uniform θ_z is readily apparent.

The growth of β is further demonstrated in figure 10, which shows values of

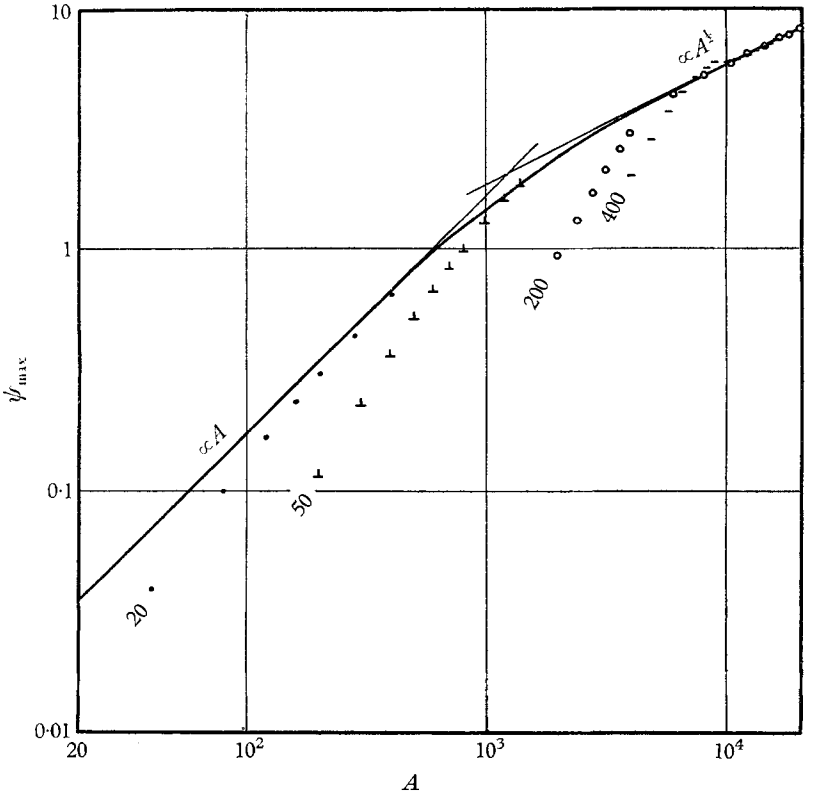

FIGURE 8. Maximum value of the stream function, ψ_{max} as a function of the Rayleigh number, A. Also shown, the solution for ramps 0 (ΔA) A of various ΔA.

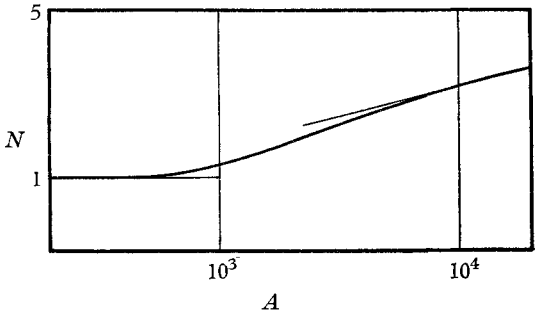

FIGURE 9. Nusselt number N as a function of the Rayleigh number A.

βh as a function of A for slots of various h. We notice for the lower values of A that $\beta \propto A^2$, the data of figure 10 giving crudely

$$\beta h^3/A^2 \doteqdot 8 \times 10^{-7}. \tag{14a}$$

There is a pronounced overshoot of about 50 % before the asymptotic value

$$\beta h \sim 0{\cdot}50 \pm 0{\cdot}01 \tag{14b}$$

is approached.

The discussion of the origin of β in Elder (1965) was largely for the case $h \gg 1$. This restriction is seen to be unnecessary.

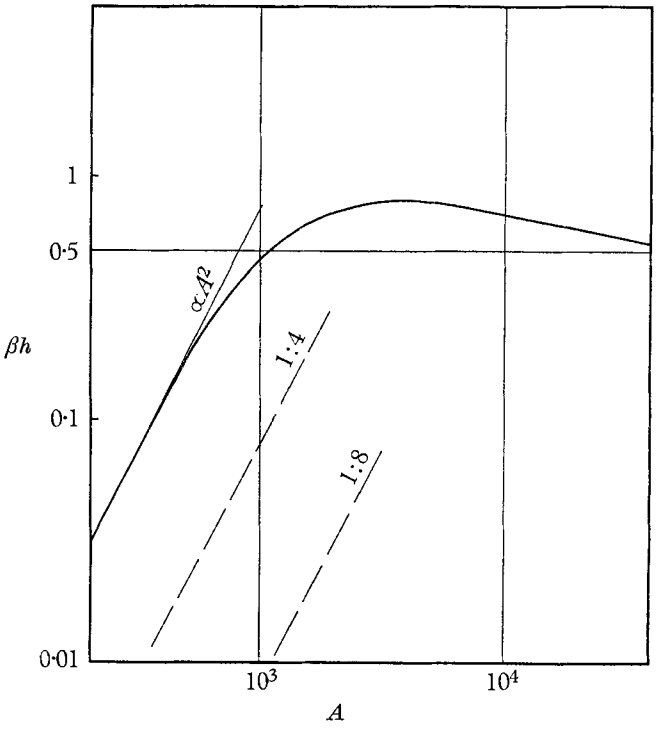

FIGURE 10. Vertical temperature gradient; βh as a function of the Rayleigh number A. Broken lines are for marked values of h.

4.6. *Role of the Prandtl number*

The data showing the direct role of the Prandtl number are summarized in figures 11, 12.

Figure 11 shows $\psi_{\max}(A)$ for two values of $\sigma = 1, 10^3$. As is to be expected we see that for small values of A ($\lesssim 200$) the solution is in the linear region and is independent of σ. There is, however, a small effect in the boundary-layer region. Figure 12 is an attempt to show directly the role of σ on ψ and N in the boundary-layer region. The data for $\sigma \gtrsim 1$ is reliable to about $\pm 0{\cdot}1$ %, but below $\sigma = 0{\cdot}1$ the uncertainty increases rapidly to about ± 1 %. This is due to the increasing numerical instability and the consequent necessity to experiment at lower Rayleigh numbers. For example, at $\sigma = 10^{-2}$ stable solutions are possible

only for $A < 60$. It therefore seems likely that a study of flows at small Prandtl number would require a separate investigation with a different numerical scheme.

The most important result of the studies relating to figure 12 is that for free convective flows with $\sigma \gtrsim 1$ the role of the inertia terms is a minor one. Hence

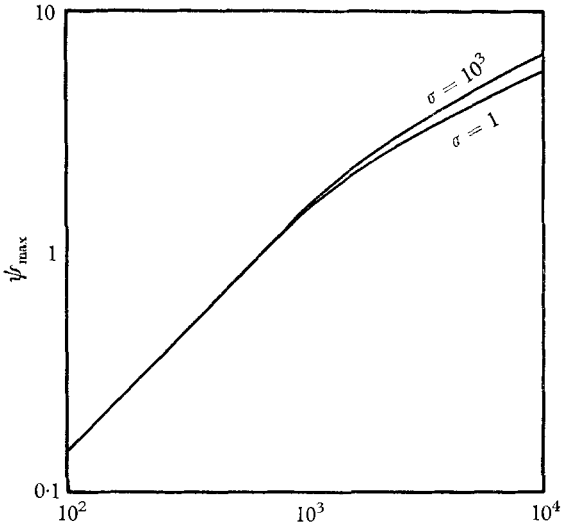

FIGURE 11. Role of the Prandtl number, ψ_{max} (A) for $\sigma = 1$, 10^3 for a ramp $A = 0$ (100) 8000 in a 11 x 11 mesh.

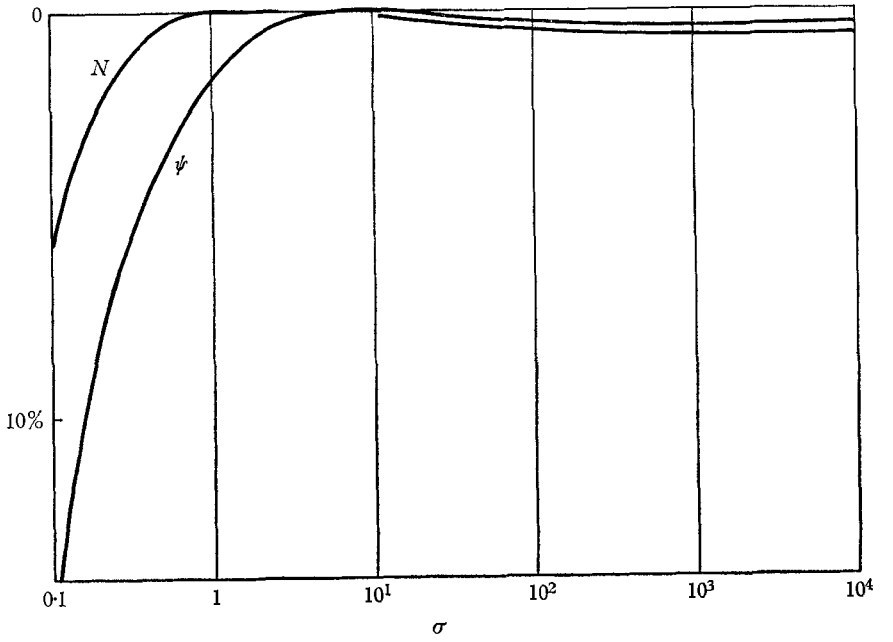

FIGURE 12. Role of the Prandtl number on ψ_{max} and N at fixed A; departure in % from maximum value. Value at $\sigma = 1$, 10, 10^2, 10^3 10^4 for a ramp $A = 0$ (200) 10^4. Other values for a logarithmic ramp $-102{\cdot}4$ (0·7071) 0·1 at $A = 2 \times 10^3$. The diagram should be regarded as schematic rather than quantitative (see text).

in theoretical studies to let $\sigma \to \infty$ is probably an excellent approximation for most common fluids, including gases. The flows with $\sigma \to \infty$ are non-linear solely through advection as is the case in a porous medium. In non-steady problems the present study suggests that $\sigma \to \infty$ is probably also an excellent approximation. In this case changes occur solely through the term $\partial\theta/\partial t$. Whether or not this approximation would be a useful one for studies of thermal turbulence is, however, not clear.

The most interesting features of figure 12 are the rapid variation for $\sigma \leqslant 1$ and that the weak maxima for N and ψ occur at quite different A (of order $A = 1$ and 10, respectively).

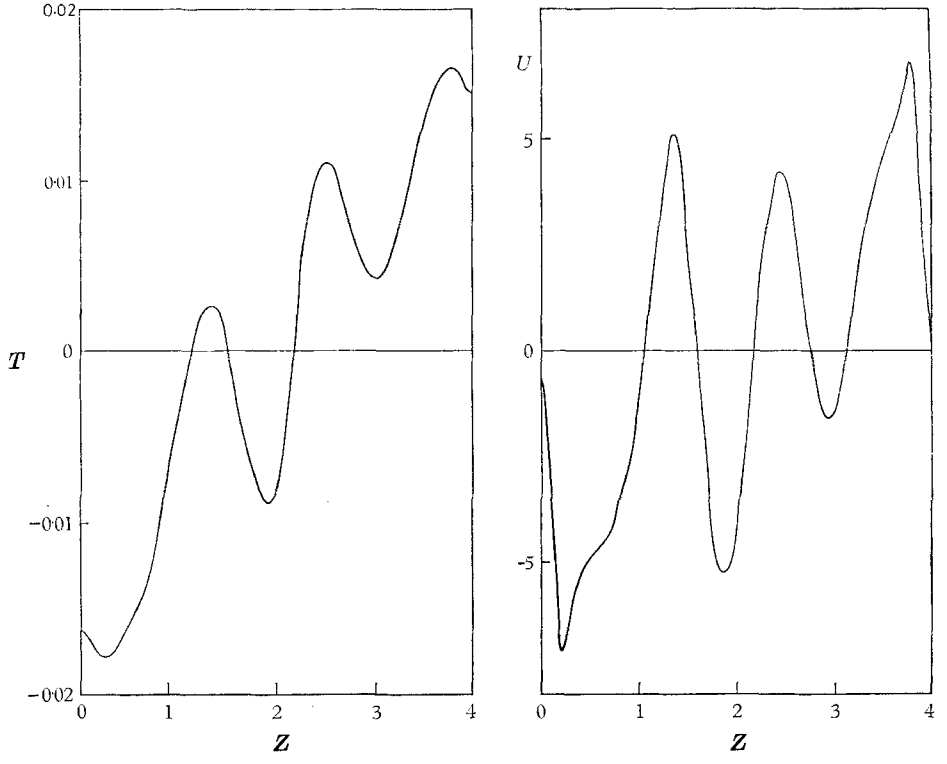

FIGURE 13. Solution in the unstable region $h = 4$, $A = 1500$, $d = \frac{1}{10}$: (*a*) Temperature on the centre line $x = \frac{1}{2}$, $T = \theta(\frac{1}{2}, z) - \frac{1}{2}$. (*b*) Entrainment velocity, $U(\frac{1}{2}, z)$.

4.7. *A speculation on some curious results in the region of numerical instability*

In the region of numerical instability some intriguing solutions have been obtained for flows in cavities with $h \geqslant 4$ prior to the solution diverging. The motions are very similar to those of the secondary flows found by Elder (1965). If I had not done those experiments, the results of this section would have been discounted. Even so, one hesitates at placing great significance on the solutions. Nevertheless, the results show certain reproducible features and are of sufficient interest to be set down.

The principal features are shown in figures 13 and 14 for solutions in a 11×41 mesh at $A = 1500$, $\sigma = 1$. The features of interest appear after about 10 scans and persist till the solution diverges after 55 scans. Figure 13 shows the temperature on the centre line together with the entrainment velocity $U(\frac{1}{2}, z)$. Figure 14 shows the corresponding vorticity. The solutions suggest the presence of a secondary flow of vertical wavelength $\approx 1{\cdot}2$.

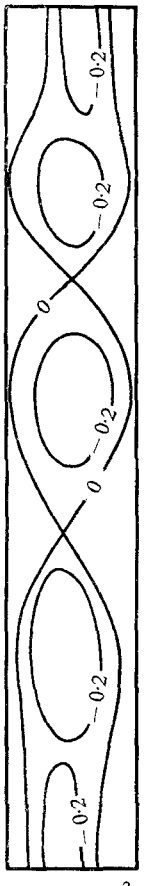

FIGURE 14. Solution in the unstable region: the vorticity (as in figure 13).

An immediate explanation of this phenomenon comes to mind when it is recalled that the outer iteration used here behaves like the time-dependent problem at large times (Garabedian 1956). In the laboratory experiments secondary flows were not observed till the Rayleigh number was somewhat above 10^4. Yet here we have flows of a similar appearance at $1{\cdot}5 \times 10^3$. The situations are, however, quite different in that here in scanning the system of equations in the region of numerical instability the system is at each step subjected to finite-amplitude disturbances (cf. figure 2). It would appear that these disturbances are capable of exciting other modes of the system, which would otherwise be strongly damped.

5. Discussion of the numerical solutions

Throughout this investigation the outstanding feature has been the ease with which the numerical programme has been able to reproduce the flows found in the laboratory. However, it is necessary to remark that this was not due to the existence of readily adaptable numerical procedures, but to the existence of a well-formulated, moderately well-understood problem.

The gross features of the flow indicated in figures 8, 9, 10, 12, are those expected. Batchelor (1954) has discussed the linear region; the boundary-layer region and in particular the vertical temperature gradient has been measured and discussed by Elder (1965).

The most interesting solutions given here are those of figures 6, 7 which show the development of the boundary layers and the fully-developed boundary-layer flow. The initial departure from the symmetry of the flow at small Rayleigh numbers occurs in the lower left- and upper right-hand corners. As the non-linear terms increase they gradually dominate over diffusion. For example, in figure 7 the contribution to the vorticity source term U which comes from advection of vorticity reaches locally 92%. The non-linear terms become strongly localized sources. This is especially so for the inertia. Terms further down the sequence (3*a–e*) are smoother, due to the predominant role of diffusion.

It is of interest to compare some of the predictions of the simple theory of Elder (1965) with those of the numerical solutions. Consider for example result (13*b*). From equation (11*b*) of Elder (1965) we find that the Nusselt number N' evaluated at $z = \frac{1}{2}h$, $x = 0$ or 1 is

$$N' = 0{\cdot}30\,(A/h)^{\frac{1}{4}}, \tag{15}$$

(where throughout we take $f = 0{\cdot}5$ and $\beta = 0{\cdot}5/h$). The numerical results show that the mean Nusselt number N differs from N' at most by 5% so that (13*b*) and (15*c*) are comparable. They differ by 20% and only a few percent of this could be due to numerical inaccuracy. Further, consider the predicted values of the vertical velocity. From equation (11*a*) of Elder (1965) we find that the maximum value of the vertical velocity satisfies

$$W_{\max}/(Ah)^{\frac{1}{2}} = K, \tag{16}$$

where $K = 0{\cdot}23$. From the data of figure 7 we find that with $h = 1$, $A = 2 \times 10^4$, $W_{\max} = 37{\cdot}5$ so that $K = 0{\cdot}27$. Hence the simple theory is 16% high. It can be concluded that the theory of Elder is at best accurate to 10%. It is surprising that the theory works so well for it only purports to describe the interior region between the boundary layers and not the form of the boundary layers themselves. The inadequacies of the simple theory are largely removed in a recent investigation by Gill (1965).

The numerical scheme has proved very convenient and rapid and has produced results comparable in accuracy with the best laboratory measurements. It can be anticipated that other non-linear elliptic problems could be solved in a similar way. It should be remarked that the human effort involved in solving numerically a *well-formulated* problem is an order of magnitude less than a similar laboratory

investigation. Unfortunately, with present day computing machines the solutions are limited to only moderately non-linear problems. A solution, for example, of the time-dependent problem for turbulent motion is probably out of the question at the moment.

In most of the analytical work on this and similar problems, little has been done for flows intermediate in behaviour from that of the weak nearly linear flows and the fully-developed boundary-layer flows. Yet as seen here this is a region well suited to present-day computing machines. But we have not learned any strikingly new physics, although that is to be expected. The mechanisms which govern laminar free convection: the torque due to the horizontal gradient of buoyancy forces, diffusion and advection of vorticity and heat, are reasonably well understood. Nevertheless, our conceptual framework for treating essentially non-linear problems, clearly indicated when we attempt to predict the behaviour of a new system, is very poor and we have barely begun to realize the vision of such men as John von Neumann.

I wish to acknowledge my debt to the members of the University of California, San Diego Computing Center and to their superb facility. Dr Clay Perry kindly read and commented on a draft of this paper. This work was supported by a National Science Foundation Grant GP-2414 and an Office of Naval Research Contract Nonr-2216.

REFERENCES

BATCHELOR, G. K. 1954 *Quart. Appl. Math.* **12**, 209.

ECKERT, E. R. G. & CARLSON, W. O. 1961 *Int. J. Heat & Mass Transfer*, **2**, 106.

ELDER, J. W. 1965 *J. Fluid Mech.* **23**, 77.

FOX, L. 1962 *Numerical Solution of Ordinary and Partial Differential Equations.* London: Pergamon Press.

FROMM, J. E. & HARLOW, F. H. 1963 *Phys. of Fluids*, **6**, 975.

GARABEDIAN, P. R. 1956 in *Math .Tables Aids Comput.* **10**, 183.

GILL, A. E. 1966 (To be published.)

GOLDSTEIN, S. 1938 (Ed.) *Modern Developments in Fluid Dynamics.* Oxford University Press.

LOVE, A. E. H. 1927 *Mathematical Theory of Elasticity.* Cambridge University Press.

PEACEMAN, D. W. & RACHFORD, H. H. 1955 *J. Soc. Indust. Appl. Math.* **3**, 28.